36th International Electric Vehicle Symposium and Exhibition (EVS36)
Sacramento, California, USA, June 11-14, 2023

Experimental Investigation of Desiccant-Coated Heat Exchanger for Electric Vehicles

Tomohiro Higashi[1], Li Zhang[1], Atsushi Inaba[2], Haruyuki Nishijima[2], Michiyuki Saikawa[1]

[1]*Central Research Institute of Electric Power Industry, 2-6-1 Nagasaka, Yokosuka-shi, Kanagasa 240-0196 Japan, higashi3808@criepi.denken.or.jp*

[2]*Denso Corporation*

Executive Summary

One of the problems for EVs is the reduction of cruising range during the heating operation of air-conditioning. A novel EV air-conditioning system that combines a heat pump and a desiccant-coated heat exchanger (DCHE) has been proposed. This system reduces the heating load and energy consumption by dehumidifying cabin air for anti-fogging the windshield by DCHE. In this research, the performance of DCHE was experimentally investigated, and the results were applied to predict the system performance. The system could reduce heating energy consumption by 81.1% compared with the conventional air-condintioning system, which can enhance the cruising range.

Keywords: Electric vehicle (EV), Air conditioning, heat pump, energy consumption, heating

1 Background

Electric vehicles (EVs) are attracting attention in response to tighter environmental regulations worldwide; however, one of the factors hindering their widespread use is the reduced cruising range by heating the cabin (air-conditioning) [1]. EVs do not have exhaust heat from the internal combustion engine (ICE); therefore, they require additional energy consumption for heating, which directly leads to a decrease in the cruising range. Another problem is fogging on the inside of the windshield during the winter. In general heating systems, dry ambient air is dehumidified using a refrigeration cycle and then heated again to be supplied to the windshield to prevent fogging; however, introducing the ambient air at a low temperature to the cabin further increases the heating load [2]. To overcome the issue, several systems have been investigated such as vapor compression heat pump system [3], refrigerant injection system [4], adsorption air conditioning system [5], and heat storage heating system [6].

The authors have proposed a novel air conditioning system that combines a heat pump cycle with a desiccant that adsorbs moisture [7]. The system can reduce heating power consumption by reducing the amount of ventilation. Fig. 1 shows a schematic diagram of the system. The system consists of an inside heat exchanger (HEi), a desiccant-coated heat exchanger (DCHE), an outside heat exchanger (HEo), a compressor, refrigerant circuit switching valves, expansion valves, and air dampers. During heating operation, the system operates two modes alternately: an internal air mode (Int. mode) and a ventilation mode (Vent. mode). In Int. mode, HEi operates as a condenser, HEo as an evaporator, and DCHE as an evaporator. DCHE dehumidifies the cabin air by adsorption; HEi heats the air for heating operation. By supplying dry air to the windshield,

the system can realize anti-fogging operation without introducing ambient air, thereby reducing the heating load. In the Vent. mode, DCHE acts as a condenser and is regenerated by ambient air. The heated air by HEi is supplied to the cabin. This allows heating and anti-fogging while the DCHE is regenerated. The numerical analysis has been carried out, and it revealed that the proposed system can save more energy compared to conventional heat pump system.

In this research, the performance of DCHE was experimentally investigated to evaluate the feasibility of the system.

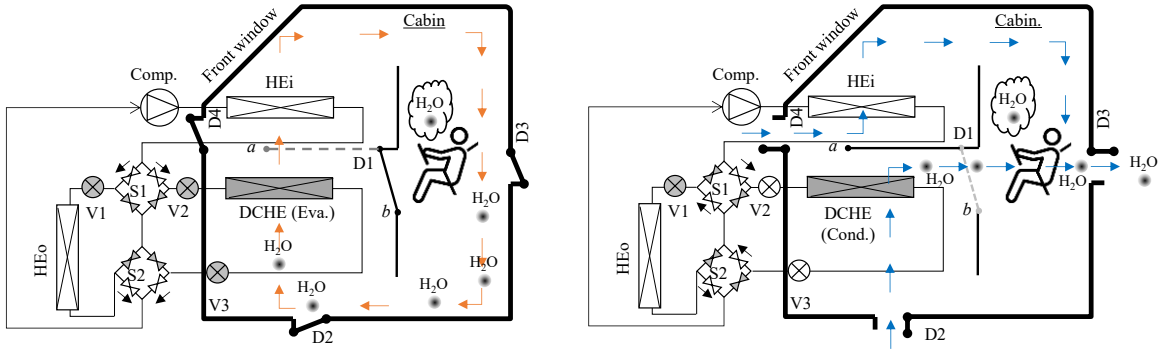

(a) Internal air mode (b) Ventilation mode

Figure 1: Schematic diagram of proposed EV air-conditionig system
HEi: inside heat exchanger, DCHE: desiccant-coated heat exchanger, HEo: outside heat exchanger, Comp.: compressor, S: refrigerant circuit switching valve, V: expansion valve, D: air damper

2 Methods

2.1 Desiccant-coated heat exchanger (DCHE)

Performance evaluation of DCHE was carried out to predict the system performance. Fig. 2 shows the external appearance of the DCHE used in this research. The DCHE is a fin-tube heat exchanger; 242mm high and 300mm wide, coated with 354.7g of FAM-Z05 (zeolite-based desiccant). The adsorption isotherm of FAM-Z05 is shown in Fig. 3. Properties of DCHE are listed in Table 1.

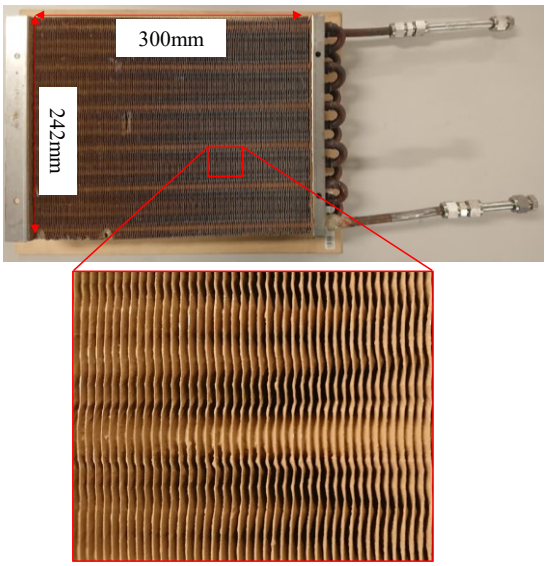

Figure 2: Overview of desiccant-coated heat exchanger (DCHE)

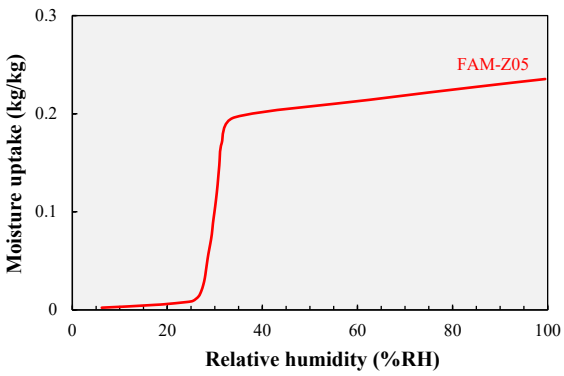

Figure 3: adsorption isotherm of FAM-Z05

Table 1: Properties of DCHE

Parameters	Values
Height (mm)	242
Width (mm)	300
Depth (mm)	50.8
fin pitch (mm)	1.8
A_f (m^2)	1.93
A_t (m^2)	0.18
A_a (=A_f+A_t) (m^2)	2.11
Desiccant	Zeolite-type sorbent FAM-Z05
Amount of desiccant (g)	750
Coating rate (g· m^{-2})	354.7

2.2 Experimental apparatus

A wind tunnel apparatus was used to test the DCHE. Figs. 4 and 5 show the exterior view and the schematic diagram of the apparatus, respectively. The apparatus consists of two air supply sources, two brine supply sources, a test section containing the heat exchanger, and measurement equipment. One of the supply sources generates adsorption air, and the other generates desorption air. The air temperature, humidity, and airflow rate are controlled respectively. Only one of the two air is supplied to the test section by switching the dampers. Similarly for brine, two brine sources are used for adsorption and desorption, respectively. The temperature and flow rate are controlled, and one of the brines is supplied to the heat exchanger by switching valves. Ethylene glycol antifreeze was used as the brine. Fig. 6 shows the appearance of the test section The test section has an air rectifier, and several sensors to measure the temperature and humidity at the air inlet/outlet.

Figure 4: Exterior view of the wind tunnel apparatus

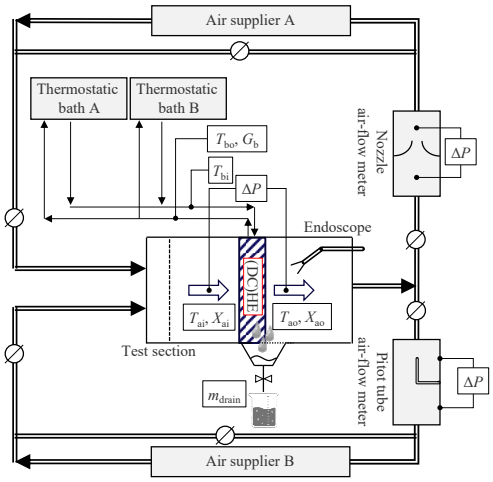

Figure 5: Schematic diagram of the wind tunnel apparatus

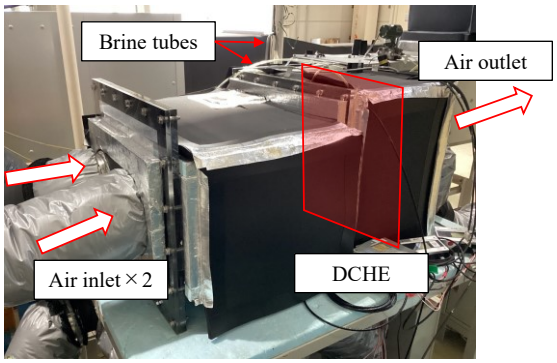

Figure 6: Test section

2.3 Experimental conditions

Experimental conditions were calculated in the following ways;

1. Assume an inside temperature (T_{cab}) and an ambient temperature (T_{amb}).
2. Calculate the temperature inside the windshield (T_{gi}) from the thermal conductivity and the heat transfer coefficient of the windshield.
3. Calculate the saturated absolute humidity (X_{gi}) at T_{gi}. Note that a lower humidity than X_{gi} can prevent fogging at the windshield.
4. Calculate the humidity in the cabin (X_{cab}) from X_{gi}. T_{cab} and X_{cab} are now experimental conditions.

Table 1 lists the experimental conditions. Two ambient air temperature conditions were assumed: 0°C and -10°C. Brine inlet temperature at Int. mode was varied from 25°C (isothermal adsorption), 20, 15, and 10°C (cooling adsorption). The time that the outlet air absolute humidity (X_{ao}) remains below X_{gi} (anti-fog duration) was investigated.

Table 1: Experimental conditions

Parameters	Int. mode (Adsorption AD mode)	Vent. mode (Desorption DE mode)
Air inlet temp. (°C)	25	-10, 0
Air inlet humidity (%RH)	23.3, 35.8	50
Air velocity (m· s^{-1})	1.0	1.5
Brine inlet temp. (°C)	25, 20, 15, 10	50
Brine flow rate (l· min^{-1})	5	5
time (min)	20	10

3 Results

3.1 Experimental results

Fig. 7 shows experimental results of inlet/outlet air temperature and humidity. The inlet air temperature at Vent. mode was -10 °C, and the inlet brine temperature at Int. mode was 25°C. At the Vent. mode, air at -10°C (dashed black line) was supplied to DCHE, was heated by the brine at 50°C, and the outlet air became about 35°C (dashed blue line). The outlet humidity (solid red line) increased to 4g· kgDA^{-1} at the beginning of the Vent. mode, and then gradually decreased to converge to the inlet humidity (solid green line). At the Int. mode, the inlet and the outlet air and brine temperatures were 25°C. The air was dehumidified by DCHE, and the outlet humidity was lower than the inlet. Then the outlet humidity gradually increased with the progress of adsorption, converging with the inlet humidity. The amount of adsorption/desorption (M_{ad}) was calculated by the absolute humidity difference between the inlet and the outlet (Eq. (1)). The amounts of desorption and adsorption were 51.5 g and 53.2 g, respectively. The relative error was 3.2%. The experiments were carried out with high accuracy

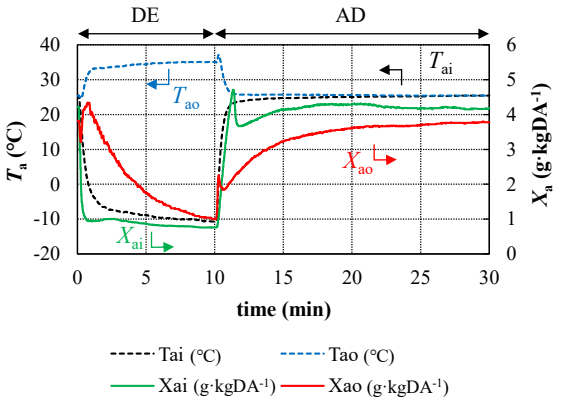

Figure 7: Change in air temperature and humidity atinlet and outlet of DCHE

$$M_{\mathrm{ad}} = \begin{cases} \int_0^{600} G_{\mathrm{a}}(X_{\mathrm{ao}} - X_{\mathrm{ai}})dt\,, & \text{(DE mode)} \\ \int_{600}^{1800} G_{\mathrm{a}}(X_{\mathrm{ai}} - X_{\mathrm{ao}})dt\,, & \text{(AD mode)} \end{cases} \tag{1}$$

Fig. 8 shows the change in the outlet air absolute humidity (X_{ao}) at different adsorption temperatures (brine inlet temperature (T_{bi}) in AD mode). The horizontal axis shows time and the vertical axis shows absolute humidity, with the AD mode (10 to 30 minutes in Fig. 7) excerpted. The red line indicates X_{gi} = 3.11 (g· kgDA^{-1}) at -10°C, and anti-fog is possible when X_{ao} is below this line. The yellow-green line; the results with 25°C of adsorption temperature, indicates that $X_{ao} < X_{gi}$ until 4'22". The anti-fog duration time under the condition was 262 seconds. The lower the adsorption temperature, the longer the anti-fog duration. The anti-fog duration was 528 seconds at an adsorption temperature of 10°C.

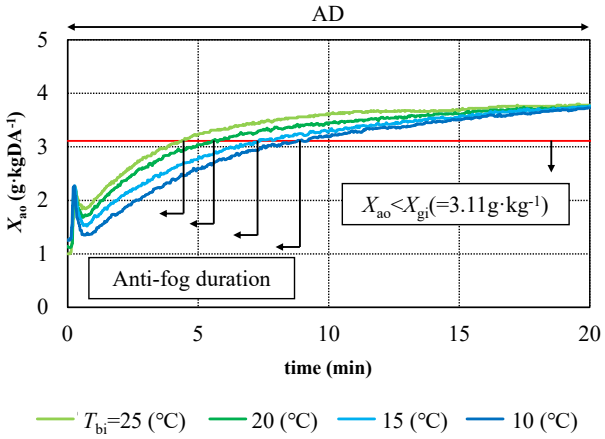

Figure 8: Absolute humidity of outlet air at different adsorption temperatures ($T_{bi,AD}$= -10°C)

The absolute humidity of the outlet air (X_{ao}) decreased to about 1.3-1.8 g· kgDA^{-1} at the start of the adsorption operation, and increased gradually thereafter. Since $X_{ao} < X_{gi} = 3.11$ (g· kgDA^{-1}) or less is sufficient for anti-fog, excessive dehumidification should be avoided for longer anti-fog duration. Therefore, the adsorption temperature control was attempted in this research by stopping the brine flow temporarily at the beginning of adsorption. , The dehumidification rate was suppressed because the DCHE was not cooled by brine with no brine flow, thereby extending the anti-fog duration. The experimental procedure is as follows.

1. The DE mode is performed as described above.
2. After DE mode, the air is switched to AD mode conditions, and the brine is stopped.
3. When X_{ao} reached X_{gi}, brine flow under AD mode condition is started.

Fig. 9 shows the experimental results with adsorption temperature control. The experimental conditions are the same as in Fig. 8, with the brine temperature at 15°C in AD mode. The blue line shows the absolute outlet air humidity (X_{ao}; excerpt from Fig. 8) when the brine flow was continued during adsorption (w/o T cont.), and the black line shows X_{ao} when the adsorption temperature was controlled by the procedure above (w/ T cont.). The results show that X_{ao} with temperature control was higher at the beginning of the AD mode because no brine was supplied and no cooling took place. When the brine flow started, X_{ao} with temperature control decreased again because of cooling by the brine. The anti-fog duration with temperature control was 8'39", which was 79 seconds longer than the results without temperature control.

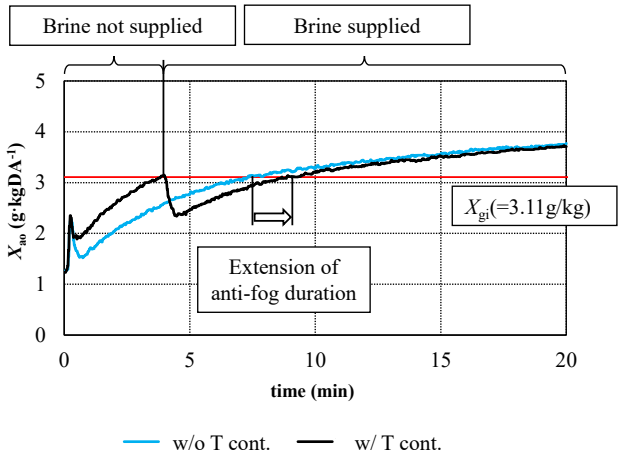

Figure 9: Extending anti-fog duration by controlling adsorption temperature ($T_{bi,AD}$ =15°C)

Fig. 10 summarizes the anti-fog duration at different adsorption temperatures ($T_{bi,AD}$) with and without temperature control. The black line shows the results at an ambient temperature (T_{amb}) of 0°C. The anti-fog duration was almost constant regardless of the adsorption temperature ($T_{bi,AD}$). On the other hand, the blue line; the results at T_{amb} of -10°C; shows that the lower the adsorption temperature, the longer the anti-fog duration. In all results, it was confirmed that the anti-fog durations were extended by 16-38% by controlling the adsorption temperature. The results indicate that the dehumidification rate can be adjusted by controlling the adsorption temperature, thereby extending the anti-fog duration.

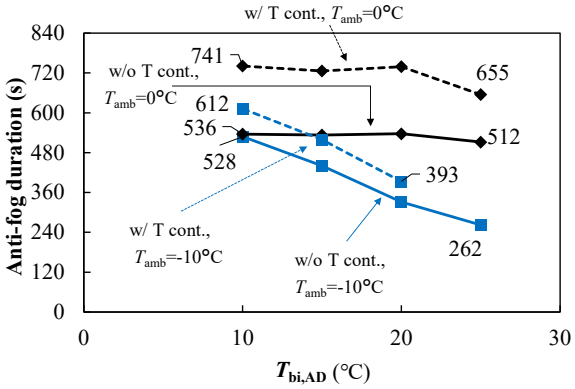

Figure 10: Relationship between adsorption temperature ($T_{bi,AD}$) and anti-fog duration
(Blue line: -10°C of ambient temperature condition, black line: 0°C of ambient temperature condition
Solid line (w/o T cont.): result of normal adsorption operation, dashed line (w/ T cont.): result with adsorption temperature control)

3.2 Performance prediction of proposed air-conditioning system

The interior heating load (Q_{cab}) (kW) was assumed to be the sum of the following three loads. Please note that only the sensible heat load was considered in all of the following.

$$Q_{cab} = Q_{amb} + Q_{ven} + Q_{pas} \tag{2}$$

- Q_{amb} (kW): Heat outflow through the car body walls and glasses. Calculated from the heat transfer rate of the walls and glasses, and the temperature difference between the inside and outside of the car.
- Q_{ven} (kW): Ventilation heat load. Calculated from the ventilation rate and the temperature difference between the inside and outside of the car. The ventilation load is 0 in the internal air mode because no ventilation is performed.
- Q_{pas} (kW): Passenger heat load. The product of sensible heat generation per person and the number of passengers. Since the heating load is considered here, the passenger heat load takes a negative value.

Table 2 and Fig. 11 show the heating load calculation conditions and heating loads at different outdoor temperatures, respectively. At an ambient temperature of -10°C, the heating load at the internal air mode and the ventilation mode were 1.20 kW and 4.68 kW, respectively. As shown here, the heating load becomes very large with ventilation. Heating energy savings can be expected by extending the internal air mode due to the dehumidification of DCHE.

Table 2: Conditions to calculate heating loeads

Parameters	Values
T_{cab} (°C)	25
Overall heat transfer coefficient of walls (kW· m^{-2}· K^{-1})	0.0014
Surface area of walls (m^2)	8
Overall heat transfer coefficient of windows (kW· m^{-2}· K^{-1})	0.011
Surface area of windows (m^2)	3
Number of passengers	5
Sensible heat load of passengers (kW· $person^{-1}$)	0.069
Air flow rate of ventilation (m^3· h)	0 (Int. mode) 300 (Vent. mode)

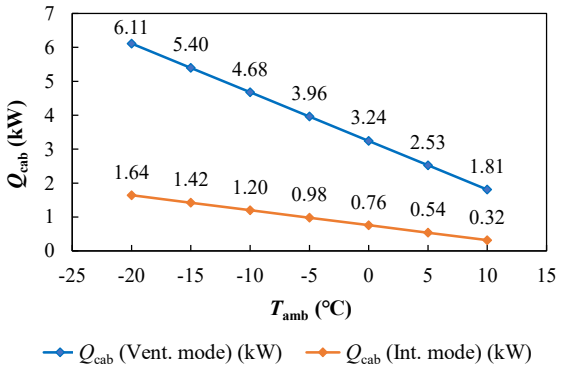

Figure 11: Heating load (Q_{cab}) at different ambient temperatures (T_{amb})

Fig. 12 shows the system heating load at different adsorption temperatures. The horizontal axis shows the adsorption temperature (T_b), and the vertical axis shows the average system heating load in internal air mode and ventilation mode. The different colors indicate the breakdown of the heating load, with (Q_{HEi}) representing the interior heat exchanger heating load, (Q_{DCHE}) representing the DCHE heating load, and ($Q_{HC,DCHE}$) representing the DCHE heat capacity load. In the internal air mode, the system heating load increased with decreasing adsorption temperature. It is because the air is cooled during adsorption, which increases the amount of heating required for the interior heat exchanger. In the ventilation mode, the total heat capacity of DCHE accounted for approximately 60% of the total heating load. The heat capacity load of DCHE is the heat used to raise the temperature of DCHE itself, and was nearly proportional to the difference in adsorption and desorption brine temperatures.

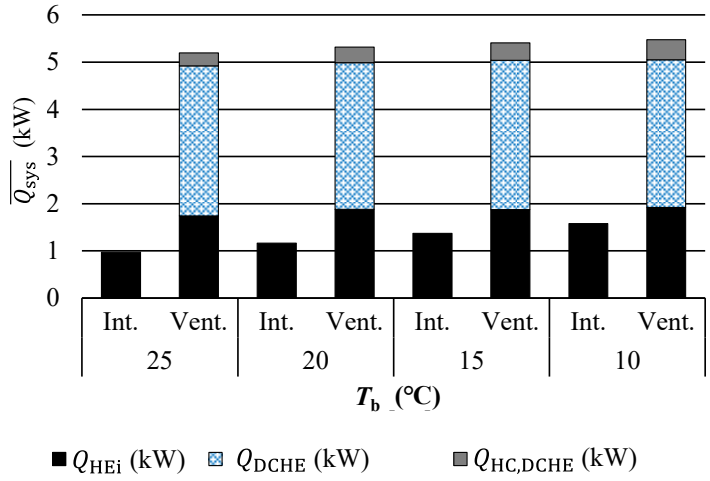

Figure 12: Average heating load ($\overline{Q_{sys}}$) of the internal air mode and ventiration mode at different adsorption temperatures (T_b)

(Ambient temperature T_{amb} =-10°C)

The total heating load was estimated assuming the DCHE was applied to the system. The latent and sensible heat treatment, anti-fog duration, and brine cooling and heating loads obtained in the experiments were used. Here, the COP of the electric heater was assumed to be 1, and that of the heat pump (HP) was determined by referring to the previous research [7]. Fig. 13 shows the average heating load (shaded area) and average power consumption (colored area) for each heating method at -10°C of the ambient air temperature. The heating load for the proposed system was 2.65 kW. The result was about 43% lower than that of the conventional air conditioning system using electric heaters (AC-heater in the figure) or heat pumps (HP-Conv in the figure), 4.86kW. It is due to the dehumidifying and anti-fogging effect of DCHE, which reduces the amount of ventilation. In addition, by combining a heat pump with a high COP, this system reduced power consumption by 81.1% compared to conventional air conditioning using an electric heater, and by 43.3% compared to conventional air conditioning using a heat pump. The results indicate that the proposed system can enhance the cruising range of EVs.

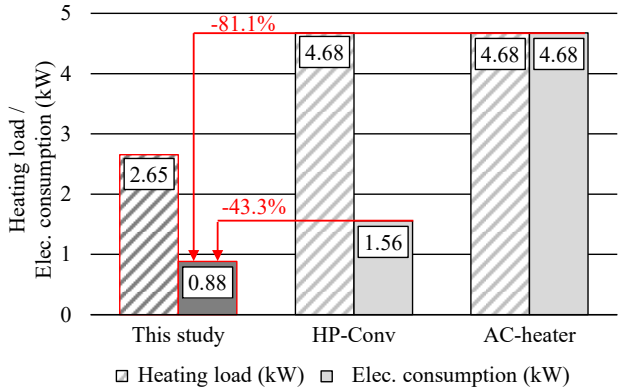

Figure 13: Comparison of heat load and Electricity consumption
(HP-Conv: Conventional heating system by heat pump
AC-heater: Heating system by electric heater)

4 Conclusion

The performance of a desiccant-coated heat exchanger (DCHE) for a novel EV air-conditioning system was experimentally investigated. This system combines the DCHE and heat pump, and can reduce the heating load and energy consumption by dehumidifying cabin air to anti-fogging the windshield. The anti-fog effect of DHCE was analyzed under several conditions. It was revealed that adsorption temperature control could enhance the anti-fog duration. The performance of the system was predicted by using the measurement results. The system could reduce the electricity consumption of heating by 81.1% compared with the conventional air-conditioning system by an electric heater, and 43.3% compared with the conventional heat pump system.

Nomenclature

AD	adsorption	
COP	coefficient of performance	
DCHE	desiccant coated heat exchanger	
DE	desorption	
G	mass flow rate	kg· s^{-1}
HE	heat exchanger	
M_{ad}	total amount of adsorption or desorption (or absorption)	g
Q	heat transfer rate	
T	temperature	°C
t	time	s
X	absolute humidity	g· $kgDA^{-1}$

Index

a	air
b	brine
cab	cabin
g	glass
HC	heat capacity
i	inlet, inside
Int.	Internal air mode
o	ouslet, outside
Vent.	Ventilation mode

References

[1] D. Yang et. AL., Recent advances on air heating system of cabin for pure electric vehicles: A review, Heliyon, 8(2022), e11032

[2] G. Zhang et. AL., Investigation on an improved heat pump AC system with the view of return air utilization and anti-fogging for electric vehicles, Applied Thermal Engineering, 115(2017), 726-735

[3] S. Daviran et. AL., A comparative study on the performance of HFO-1234yf and HFC-134a as an alternative in automotive air conditioning systems, Applied Thermal Engineering, 110(2017), 1091-1100.

[4] C. Kwon et. AL., Performance evaluation of a vapor injection heat pump system for electric vehicles, International Journal of Refrigeration, 74(2017), 138-150

[5] G. An et. AL., Study on working pairs of sorption type air conditioner for electric vehicles under different temperature zones, Journal of Thermal Science, 28(2019), 1004-1014

[6] N. Putra et. AL., Performance of beeswax phase change material (PCM) and heat pipe as passive battery cooling system for electric vehicles, Case Studies in Thermal Engineering, 21(2020), 100655

[7] L. Zhang et. AL., Performance analysis of a heat pump system with integrated desiccant for electric vehicles, International Journal of Refrigeration, 86(2018), 154-162

Presenter Biography

Tomohiro Higashi graduated with a Ph.D. course at the Graduate School of Frontier Sciences, the University of Tokyo in 2020, working at the Central Research Institute of Electric Power Industry, Japan. His work focuses specifically on heat pump, air-conditioning, and comfortability.